Metal Cation Dependence of Interactions with Amino Acids: Bond Energies of Rb^+ to Gly, Ser, Thr, and Pro

Vanessa N. Bowman, Amy L. Heaton, and P. B. Armentrout*

Department of Chemistry, University of Utah, 315 S. 1400 E. Rm 2020, Salt Lake City, Utah 84112

Received: February 9, 2010

The interactions of rubidium cations with the four amino acids (AA), glycine (Gly), serine (Ser), threonine (Thr), and proline (Pro), are examined in detail. Experimentally, the bond energies are determined using threshold collision-induced dissociation of the Rb^+(AA) complexes with xenon in a guided ion beam tandem mass spectrometer. Analyses of the energy dependent cross sections include consideration of unimolecular decay rates, internal energy of reactant ions, and multiple ion−molecule collisions. 0 K bond energies of 108.9 ± 7.0, 115.7 ± 4.9, 122.1 ± 4.6, and 125.2 ± 4.5 kJ/mol are determined for complexes of Rb^+ with Gly, Ser, Thr, and Pro, respectively. Quantum chemical calculations are conducted at the B3LYP, B3P86, and MP2(full) levels of theory with geometries and zero point energies calculated at the B3LYP level using both HW*/6-311+G(2d,2p) and Def2TZVP basis sets. Results obtained using the former basis sets are systematically low compared to the experimental bond energies, whereas the latter basis sets show good agreement. For Rb^+(Gly), the ground state conformer has the rubidium ion binding to the carbonyl group of the carboxylic acid, and a similar geometry is found for Rb^+(Pro) except the secondary nitrogen accepts the carboxylic acid hydrogen to form the zwitterionic structure. Both Rb^+(Ser) and Rb^+(Thr) are found to have tridentate binding at the B3LYP and MP2(full) levels, whereas the B3P86 slightly prefers binding Rb^+ at the carboxylic acid. Comparison of these results to those for the lighter alkali ions provides insight into the trends in binding affinities and structures associated with metal cation variations.

Introduction

The enzymatic transfer of alkali-metal cations across cellular membranes, particularly Na^+ and K^+, is necessary for maintenance of homeostasis and cellular function. Although the heavier alkali cations, Rb^+ and Cs^+, are not essential nutrients, they follow the same biological pathways as potassium and bind at the same sites.[1,2] However, their difference in mass results in different transport and accumulation rates,[3−6] sufficiently so that rubidium and cesium isotopes can be used in imaging of tissue and tumors without severe toxicity.[7]

The approach used in our lab and others to understand the binding affinity of metal ions with complicated systems is to create a "thermodynamic vocabulary" of specific pairwise interactions in small-scale systems that can be combined to provide an understanding of systems having much greater complexity.[8] Because complications resulting from solvent effects can be eliminated, measurement of gas-phase cation affinities is quantitative and has the additional advantage of reflecting the intrinsic bond strengths between alkali metal ions and peptides. Further, this is an ideal venue for detailed comparison of experimental and theoretical results, as well as to understand how such interactions vary with the identity of the metal cation.

Previously, we have studied the pairwise interactions of the alkali-metal cations, Li^+, Na^+, and K^+, with glycine (Gly),[9−11] serine (Ser),[12] threonine (Thr),[12] and proline (Pro)[13] by examining their threshold collision-induced dissociation (TCID) using guided ion beam tandem mass spectrometry. Quantitative bond dissociation energies (BDEs) were determined and found to be consistent with theoretical values predicted for the ground state conformations. Notably, recent studies of these complexes using infrared multiple photon dissociation (IRMPD) spectroscopy find that the ground state geometries of metal cation amino acid complexes can be sensitive to the metal cation identity. Although the entire sequence of alkali cations with Gly and Pro has not been examined by IRMPD,[14] such studies of M^+(Ser)[15] and M^+(Thr)[16] have found that the $M^+ = Li^+$ and Na^+ complexes are bound in a tridentate [N,CO,OH] conformer (see below for a definition of the nomenclature used), whereas spectra for $M^+ = K^+$ and Rb^+ include evidence of bidentate [COOH] conformations. Additionally, the spectra for cesiated serine and threonine complexes also include contributions from a zwitterionic [CO_2^-] conformer. At present, it is experimentally unknown how such geometrical changes influence the BDEs of these complexes.

In the work presented here, we extend our previous TCID studies to provide the first experimental values for Rb^+ binding with amino acids. Absolute BDEs of the Rb^+ (AA) complexes, where AA = Gly, Ser, Thr, and Pro, are measured using TCID in a guided ion beam tandem mass spectrometer. Quantum chemical calculations at several levels of theory are carried out to provide structures, vibrational frequencies, and rotational constants needed for analysis of the TCID data. Multiple basis sets for rubidium are explored in order to provide theoretical BDEs in good agreement with experiment. Combined, the experimental and theoretical studies achieve a quantitative understanding of various effects (e.g., chelation, electron delocalization, inductive effects, and conformational strain) on the binding strength of all four ligands with the rubidium cations and how these effects differ from those associated with the lighter alkali cations.

Experimental and Computational Section

General Experimental Procedures. Cross sections for CID of the rubidium cation−amino acid complexes are measured

10.1021/jp101264m
Published on Web 02/25/2010

using a guided ion beam tandem mass spectrometer that has been described in detail previously.[17,18] Experiments are conducted using an electrospray ionization (ESI) source under conditions similar to those described previously.[19] Briefly, the ESI is operated using a 50:50 by volume H_2O/MeOH solution with $\sim 10^{-3}$ M amino acid and RbCl (all chemicals purchased from Sigma-Aldrich), which is syringe-pumped at a rate of 0.04 mL/h into a 35 gauge stainless steel needle biased at ~2000 V. Ionization occurs over the ~5 mm distance from the tip of the needle to the entrance of the capillary, biased at ~35 V. Ions are directed by a capillary heated to 80 °C into a radio frequency (rf) ion funnel,[20,21] wherein they are focused into a tight beam. Ions exit the ion funnel and enter an rf hexapole ion guide that traps them radially. Here, the ions undergo multiple collisions ($>10^4$) with the ambient gas and become thermalized. Ions produced in the source are assumed to have their internal energies well described by a Maxwell−Boltzmann distribution of rovibrational states at 300 K, as characterized in previous experiments.[19,22−24]

Rb^+(AA) complexes are extracted from the source and mass selected using a magnetic momentum analyzer. The mass-selected ions are decelerated to a well-defined kinetic energy and focused into a rf octopole ion guide that traps the ions radially. The ion guide minimizes losses of the reactant and any product ions resulting from scattering.[25] The octopole passes through a static gas cell containing xenon, which is used as the collision gas for reasons described elsewhere.[26,27] After collision, the reactant and product ions drift to the end of the octopole where they are extracted and focused into a quadrupole mass filter for mass analysis. The ions are detected with a high voltage dynode, scintillation ion detector,[28] and the signal is processed using standard pulse counting techniques. Ion intensities, measured as a function of collision energy, are converted to absolute cross sections as described previously.[17] The uncertainty in relative cross sections is about ±5%, and that for the absolute cross sections is about ±20%. The ion kinetic energy distribution is measured to be Gaussian and has a typical fwhm of 0.1−0.2 eV (lab). Uncertainties in the absolute energy scale are about ±0.05 eV (lab). Ion kinetic energies in the laboratory frame are converted to energies in the center-of-mass (CM) frame using $E_{CM} = E_{lab}m/(m+M)$, where M and m are the masses of the ionic and neutral reactants, respectively. All energies herein are reported in the CM frame unless otherwise noted.

Thermochemical Analysis. Threshold regions of the CID reaction cross sections are modeled using eq 1

$$\sigma(E) = \sigma_0 \sum_i g_i(E + E_i - E_0)^n/E \qquad (1)$$

where σ_0 is an energy-independent scaling factor, n is an adjustable parameter that describes the efficiency of collisional energy transfer,[18] E is the relative kinetic energy of the reactants, and E_0 is the threshold for dissociation of the ground electronic and rovibrational state of the reactant ion at 0 K. The summation is over the rovibrational states of the reactant ions, i, where E_i is the excitation energy of each state and g_i is the fractional population of those states ($\sum g_i = 1$). The Beyer−Swinehart−Stein−Rabinovitch algorithm[29−31] is used to evaluate the number and density of the rovibrational states, and the relative populations g_i are calculated for a Maxwell−Boltzmann distribution at 300 K.

Several effects that obscure the interpretation of the data must be accounted for during data analysis in order to produce accurate thermodynamic information. The first involves energy broadening resulting from the thermal motion of the neutral collision gas and kinetic energy distribution of the reactant ion. This is accounted for by explicitly convoluting the model over both kinetic energy distributions, as described elsewhere in detail.[17] The second effect considers that eq 1 only models cross sections that represent products formed as the result of a single collision event. To ensure rigorous single-collision conditions, data are collected at three pressures of Xe, generally about 0.18, 0.12, and 0.06 mTorr, and the resulting cross sections are evaluated for the pressure effects and extrapolated to zero pressure when necessary.[32] The third effect arises from the lifetime for dissociation. As the size of reactant ion complexes increases, so does the number of vibrational modes of the reactant ion and thus the time for energy randomization into the reaction coordinate after collision. Thus, some energized molecules may not dissociate during the time scale of the experiment. This leads to a delayed onset for the CID threshold, a kinetic shift, which becomes more noticeable as the size of the molecule increases. These kinetic shifts are estimated by the incorporation of Rice−Ramsperger−Kassel−Marcus (RRKM) statistical theory,[33−35] which predicts the unimolecular rate of dissociation of an energized molecule (EM). Application of RRKM theory for analysis of CID thresholds has been described in detail previously,[36−38] and transforms eq 1 into eq 2.

$$\sigma(E) = (n\sigma_0/E) \sum g_i \int_{E_0-E_t}^{E} (1 - e^{-k(E^*)\tau})(E - \varepsilon)^{n-1}\, d(\varepsilon) \qquad (2)$$

Here, ε is the energy transferred from translation into internal energy of the complex during the collision, τ is the time available for dissociation ($\sim 5 \times 10^{-4}$ s as previously measured by time-of-flight studies),[18] E^* is the internal energy of the EM after the collision, i.e., $E^* = \varepsilon + E_i$, with n, g_i, E_i, E_0, and E defined above. The term $k(E^*)$ is the unimolecular rate constant for dissociation of the EM as defined in eq 3

$$k(E^*) = dN_{vr}^{\dagger}(E^* - E_0)/h\rho_{vr}(E^*) \qquad (3)$$

where d is the reaction degeneracy, h is Planck's constant, $N_{vr}^{\dagger}(E^* - E_0)$ is the sum of rovibrational states of the transition state (TS) at an energy $E^* - E_0$, and $\rho_{vr}(E^*)$ is the density of rovibrational states of the EM at the available energy, E^*. In the limit that $k(E^*)$ is faster than the time-of-flight of the ions, the integration in eq 2 recovers eq 1.

To evaluate the rate constants in eq 3, vibrational frequencies and rotational constants for the EM and all TSs are required. Because the metal−ligand interactions in the complexes studied here are mainly long-range electrostatic interactions (ion−dipole, ion−quadrupole, and ion−induced dipole interactions), the most appropriate model for the TS is generally a loose association of the ion and neutral ligand fragments,[9,10,39−42] even for multidentate ligands.[43−46] Therefore, the TSs are treated as product-like, such that the TS frequencies are those of the dissociated products. The transitional frequencies are treated as rotors, a treatment that corresponds to a phase space limit (PSL), as described in detail elsewhere.[38,47] The 2-D external rotations are treated adiabatically but with centrifugal effects included.[48] In the present work, the adiabatic 2-D rotational energy is treated using a statistical distribution with an explicit summation over all possible values of the rotational quantum number.[38]

The model cross sections of eq 2 are convoluted with the kinetic energy distribution of the reactants and compared to the

data. A nonlinear least-squares analysis is used to provide optimized values for σ_0, n, and E_0. The uncertainty associated with E_0 is estimated from the range of threshold values determined from different data sets with variations in the parameter n, variations in vibrational frequencies (±10% for all frequencies), changes in dissociation time by factors of 2, and the uncertainty of the absolute energy scale, 0.05 eV (lab).

In deriving the final optimized bond dissociation energies (BDEs) at 0 K, two assumptions are made. First, it is assumed that there is no activation barrier in excess of the endothermicity for the loss of the ligand, which is generally true for ion−molecule reactions and for the heterolytic noncovalent bond dissociations considered here.[49] Second, the measured threshold E_0 values for dissociation are from ground-state reactant ion to ground-state ion and neutral ligand products. Given the relatively long experimental time frame (~5×10^{-4} s), incipient products should be able to rearrange to their low-energy conformations after collisional excitation.

Computational Details. Ground state conformers of the four amino acids calculated at the levels of theory discussed below have been described previously.[9,12,13] All likely conformers of serine and threonine complexed with Rb^+ have also been examined in previous work,[15,16] using the same methods as those described here for the glycine and proline complexes. For Rb^+(Gly) and Rb^+(Pro) complexes, all conformations considered previously for K^+(Gly)[10] and K^+(Pro)[13] were used as starting points for geometry and vibrational frequency calculations. These prior calculations were performed using density functional theory (DFT) at the B3LYP/6-311+G(d,p) level.[50−52] This level of theory has been shown to provide reasonably accurate structural descriptions of comparable metal−ligand systems.[9,10,13,15,16,23,53,54] For the rubidium bound complexes, the geometry and vibrational calculations are optimized at the B3LYP/HW*/6-311+G(d,p) level, where HW* indicates that Rb was described using the effective core potentials (ECPs) and valence basis sets of Hay and Wadt[55] (equivalent to the LANL2DZ basis set) with a single d polarization function (exponent of 0.24) included.[56] Relative energies are determined using single point energies at the B3LYP, B3P86, and MP2(full) levels using the HW*/6-311+G(2p,2d) basis set. Zero-point vibrational energy (ZPE) corrections were determined using vibrational frequencies calculated at the B3LYP/6-311+G(d,p) level scaled by a factor of 0.9804.[57] Basis set superposition errors (BSSEs) were estimated using the full counterpoise (cp) method.[58,59] For the MP2 single-point energies, the BSSE corrections range from 6 to 14 kJ/mol, whereas, for the B3LYP and B3P86 single-point energies, they range between 0 and 1 kJ/mol for all structures examined here. It has been previously mentioned that the full counterpoise approximation to BSSE can provide worse agreement with experiment than theoretical values without BSSE corrections.[60−63] Because of this tendency for BSSE to overcorrect for the MP2 calculations, the "best" MP2 values may fall between the MP2 values with and without the BSSE corrections, and therefore both values are reported here. All of the absolute binding energies obtained using DFT calculations reported here include cp corrections.

Although the reasonableness of the Hay−Wadt ECP/valence basis sets has been confirmed previously by performing similar HW* calculations on K^+(Ser) complexes[15] (exponent of 0.48 for the d polarization function on K),[56] the present absolute bond energies determined using this basis set do not agree with experiment particularly well (see below). Therefore, calculations were repeated for at least the three lowest energy conformers of each complex using the Def2TZVP basis set on all of the atoms.[64] This is a balanced basis set on all atoms at the triple-ζ level including polarization functions and uses an ECP on rubidium developed by Leininger et al.[65] Geometry optimizations and vibrational frequencies were calculated at the B3LYP/Def2TZVP level, with zero point energies being scaled by 0.98. Single point energies at this level as well as B3P86/Def2TZVP and MP2(full)/Def2TZVP levels using the B3LYP geometries were also calculated. BSSE corrections at the full counterpoise level were applied in all cases and ranged from 1 to 3 kJ/mol for the DFT calculations and 5 to 12 kJ/mol for the MP2(full) results. The Def2TZVP basis set was obtained from the EMSL basis set exchange library.[66,67]

Results

Cross Sections for Collision-Induced Dissociation. Kinetic-energy-dependent experimental cross sections were obtained for the interaction of Xe with Rb^+(AA), where AA = Gly, Pro, Ser, and Thr. Figure 1 shows representive data sets for all four Rb^+(AA) systems. The data shown are a mean of results taken at xenon pressures of ~0.06, 0.12, and 0.20 mTorr, as no pressure dependence for these systems was observed. For all four complexes, the only dissociation pathway observed was the loss of the intact ligand in the collision-induced dissociation (CID) reaction (4).

$$Rb^+(AA) + Xe \rightarrow Rb^+ + AA + Xe \qquad (4)$$

The model of eq 2 was used to analyze the thresholds for reaction 4 for the four Rb^+(AA) systems. Figure 1 shows that all experimental cross sections are reproduced by eq 2 over a large range of energies (>2 eV) and magnitudes (>2 orders of magnitude). The optimized fitting parameters of eq 2 are provided in Table 1. Modest kinetic shifts are observed and range from only 0.03 eV for Rb^+(Gly), the most weakly bound system, to about 0.11 eV for Rb^+(Thr), the floppiest and nearly most strongly bound system. The values of $\Delta S^{\ddagger}_{1000}$, the entropy of activation at 1000 K, are also derived, which gives some idea of the looseness of the transition states. These values, listed in Table 1, are in the range determined by Lifshitz[68] for simple bond cleavage dissociations. This is reasonable considering that the TS is assumed to lie at the centrifugal barrier for the association of Rb^+ + AA.

Theoretical Results. Structures of complexes of the four neutral amino acids with Rb^+ experimentally studied here were calculated as described above. Figure 2 shows the two lowest energy conformations for each system, and Table 2 provides more complete geometric and energetic information. Previous work has discussed the structures of the Rb^+(Ser) and Rb^+(Thr) complexes,[15,16] so only an abbreviated discussion is provided here. The nomenclature adopted here identifies the binding sites of the metal ion in brackets, augmented by other designations when required to differentiate conformers. For Rb^+(Gly), this is achieved by noting the approximate dihedral angles of ∠HOCC and ∠OCCN (designated as c for cis, <50°, and t for trans, >135°). For Rb^+(Pro), there are two similar conformations that differ only in whether the C3 carbon of the ring (C_γ) is puckered toward the carboxylic acid (or carboxylate) group, designated as C3up, or puckered away, C3down, Figure 2.

B3LYP geometries calculated using the HW*/6-311+G(2d,2p) and Def2TZVP basis sets are similar. Rubidium−ligand bond distances calculated with the latter are systematically shorter by 0.06−0.08 Å for all Rb^+−OC bonds, 0.06−0.09 Å for Rb^+−N bonds, ~0.06 Å for Rb^+−O bonds in zwitterionic

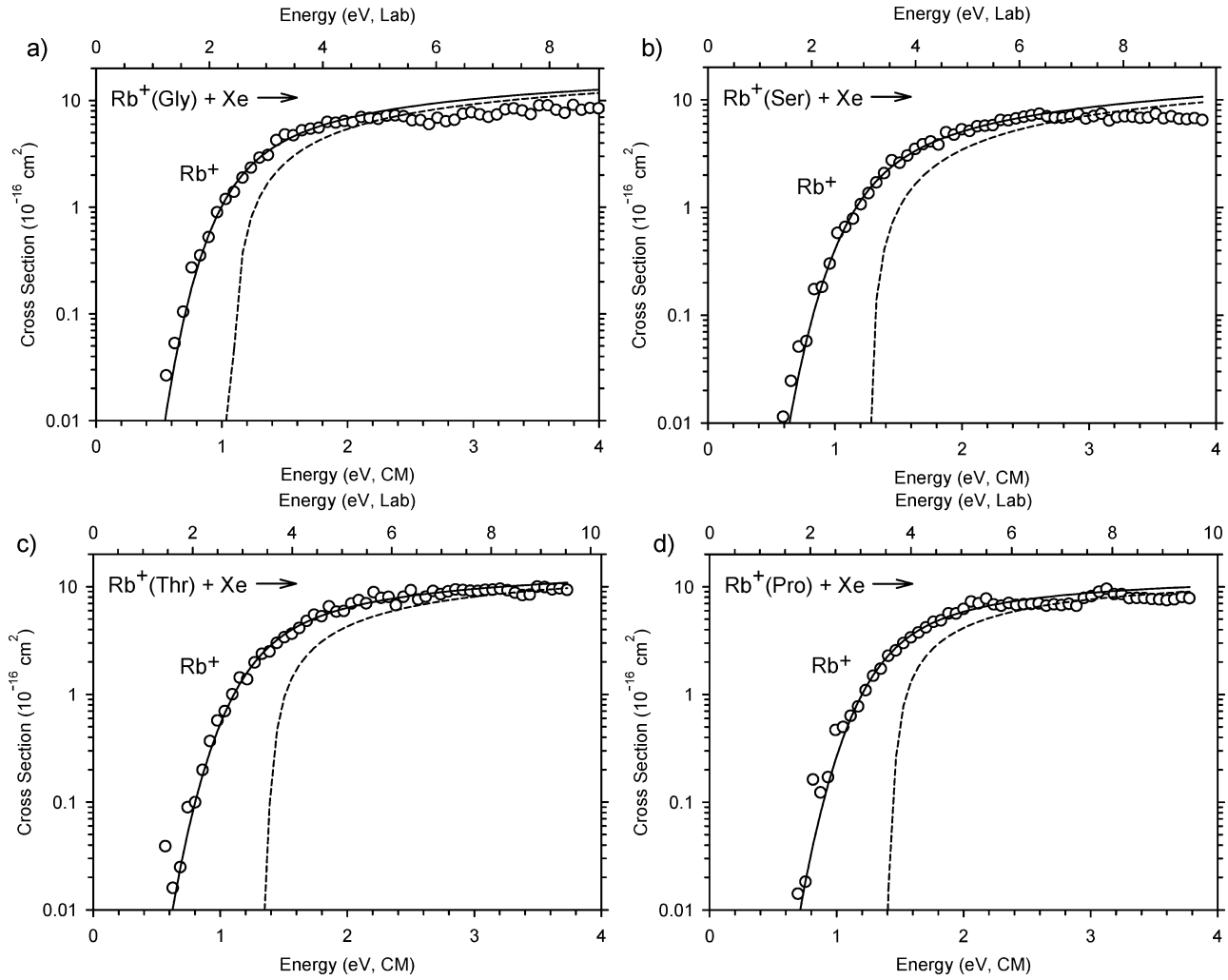

Figure 1. Cross sections for collision-induced dissociation of Rb^+(Gly), Rb^+(Ser), Rb^+(Thr), and Rb^+(Pro) (parts a−d) with xenon as a function of kinetic energy in the center-of-mass frame (lower *x* axis) and the laboratory frame (upper *x*-axis). Solid lines show the best fit to the data using the model of eq 2 convoluted over the neutral and ion kinetic and internal energy distributions. Dashed lines show the model cross sections in the absence of experimental kinetic energy broadening for reactant ions with an internal energy of 0 K.

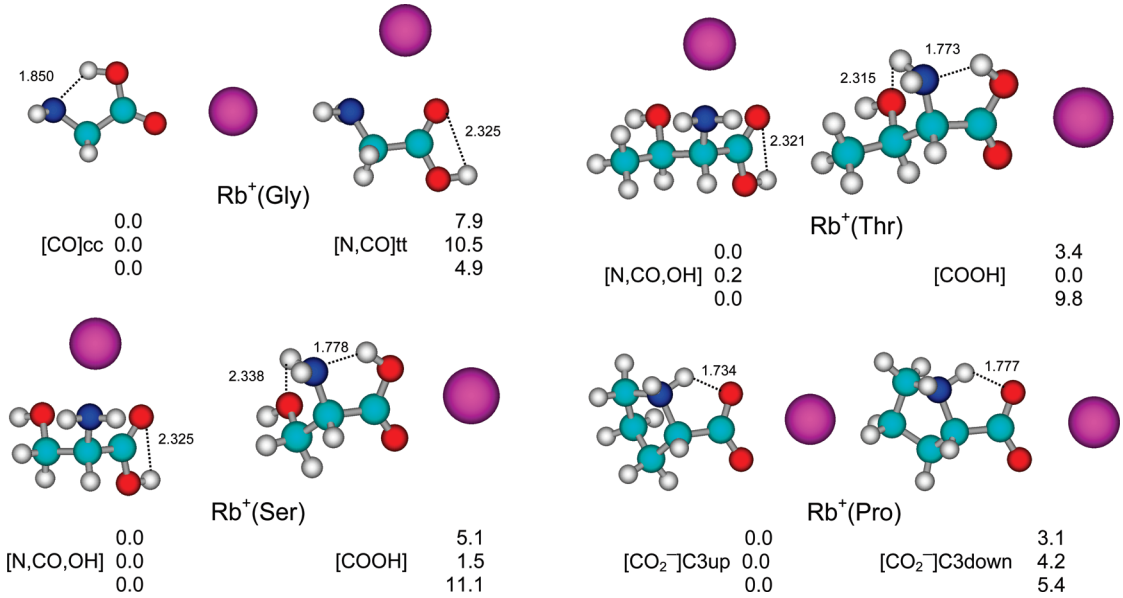

Figure 2. Rb^+(AA) low-energy structures calculated at the B3LYP/Def2TZVP level. Dashes indicate hydrogen bonds with lengths shown in Å. Relative energies in kJ/mol calculated at the B3LYP (top), B3P86 (middle), and MP2(full) (bottom) levels of theory using the Def2TZVP basis sets are shown.

TABLE 1: Fitting Parameters of eq 2, Threshold Dissociation Energies at 0 K, and Entropies of Activation at 1000 K for CID of Rb^+(AA)[a]

reactant	σ_0	n	E_0 (eV), no RRKM	E_0 (PSL) (eV)	$\Delta S^{\ddagger}_{1000}$ (J/K mol)
Rb^+(Gly)	12.4 (0.9)	1.1 (0.2)	1.16 (0.07)	1.13 (0.07)	20 (2)
Rb^+(Ser)	9.9 (1.1)	1.4 (0.2)	1.27 (0.05)	1.20 (0.05)	40 (2)
Rb^+(Thr)	13.9 (1.0)	1.2 (0.2)	1.38 (0.10)	1.27 (0.05)	41 (2)
Rb^+(Pro)	13.7 (1.3)	1.3 (0.2)	1.38 (0.05)	1.30 (0.05)	31 (2)

[a] Uncertainties in parentheses.

structures, and 0.03−0.06 Å for Rb^+−OH bonds. Relative energies calculated using the HW*/6-311+G(2d,2p) and Def2TZVP basis sets show similar trends, Table 2, with differences of 0−3 kJ/mol for the B3LYP and B3P86 single point energies and 0−5 kJ/mol for the MP2(full) results.

At all levels of theory, the ground state (GS) of Rb^+(Gly) is a structure in which the metal ion binds to the carbonyl and there is a strong OH···N hydrogen bond between the carboxylic acid group and the amine. This [CO]cc structure is much lower in energy than the alternative [CO]tc and [CO]ct structures by 33−41 kJ/mol, Table 2. The [CO]tc structure has a OH···OC hydrogen bond and two long-range NH···OH interactions, whereas the [CO]ct structure has only two long-range NH···OC interactions. The lowest excited conformer for Rb^+(Gly) is [N,CO]tt, in which the metal ion binds to both the carbonyl and amine groups of the backbone and there is an OH···OC hydrogen bond as well, Figure 2. This lies 5−12 kJ/mol above the [CO]cc ground state, whereas the alternate [N,CO]ct conformer, which no longer has the OH···OC hydrogen bond, lies another 20−21 kJ/mol higher in energy. Likewise, the [N,OH]tc conformer, in which the metal ion binds the hydroxyl group rather than the carbonyl, lies 31−39 kJ/mol higher than [N,CO]tt. The zwitterionic [CO_2^-]cc structure binds the metal ion more evenly between the two oxygen atoms of the carboxylate group (where the oxygen forming a hydrogen bond with the NH_3^+ group has a longer Rb^+−O bond by ∼0.13 Å). As the proton is transferred back to the carboxylate group, the

TABLE 2: Bond Distances (Å), Bond Angles (deg), and Relative Free Energies (kJ/mol) at 0 and 298 K for Low-Energy Structures of Rubidium-Cation-Bound Gly, Ser, Pro, and Thr[a]

								relative energies		
species	structure	$r(Rb^+-OC)^b$	$r(Rb^+-X)$	$r(Rb^+-O)^c$	$\angle XRb^+O^b$	$\angle XRb^+O^c$	$\angle O^bRb^+O^c$	B3LYP[d]	B3P86[d]	MP2(full)[d]
Rb^+(Gly)	[CO]cc	2.780,			27.2,			0.0 (0.0)	0.0 (0.0)	0.0 (0.0)
		2.712			*28.0*[f]			*0.0 (0.0)*	*0.0 (0.0)*	*0.0 (0.0)*
	[N,CO]tt	2.844,	3.222,		54.8,			9.7 (6.8)	12.4 (9.5)	5.4 (2.5)
		2.778	*3.156*[e]		*56.1*[e]			*7.9 (5.0)*	*10.5 (7.6)*	*4.9 (2.0)*
	[CO_2^-]cc	2.878,	2.998,		45.1,			19.8 (16.3)	18.0 (14.5)	14.9 (11.4)
		2.801	*2.942*[f]		*46.1*[f]			*18.5 (15.0)*	*16.8 (13.3)*	*10.3 (6.8)*
	[N,CO]ct	2.806,	3.328,		47.9,			28.8,	31.2,	25.0,
		2.745	*3.241*[e]		*54.5*[e]			*27.6*	*30.2*	*26.1*
	[CO]tc	2.787,			8.9,			33.2,	37.0,	34.0,
		2.720			*8.4*[f]			*35.0*	*38.6*	*37.4*
	[CO]ct	2.817,			29.2,			36.1,	39.1,	36.0,
		2.746			*29.6*[f]			*37.4*	*40.7*	*40.2*
	[N,OH]tc	2.968	3.108[e]		54.6[e]			45.1	48.8	35.7
	[N]tt		3.077[e]					47.3	50.0	43.0
Rb^+(Ser)	[N,CO,OH]	2.919,	3.134,	3.011,	54.3,	56.2,	66.7,	0.0 (1.0)	1.0 (4.1)	0.0 (0.0)
		2.854	*3.073*[e]	*2.964*	*55.5*[e]	*57.1*[e]	*67.9*	*0.0 (0.0)*	*0.0 (1.6)*	*0.0 (0.0)*
	[COOH]	2.907,	3.103,		42.3,			2.1 (0.0)	0.0 (0.0)	11.0 (7.8)
		2.825	*3.075*[f]		*43.9*[f]			*5.1 (2.0)*	*1.5 (0.0)*	*11.1 (8.0)*
	[CO_2^-]	2.893,	2.942,		45.5,			10.6 (10.5)	7.4 (9.3)	20.4 (19.2)
		2.811	*2.887*[f]		*46.5*[f]			*12.0 (10.1)*	*7.4 (7.1)*	*16.0 (14.1)*
	[CO,OH]	2.771		3.022	60.9[f]			12.1 (10.0)	12.0 (12.0)	23.0 (19.9)
	[N,CO]	2.822	3.177[e]		54.8[e]			13.0 (11.5)	14.0 (14.7)	20.2 (17.7)
Rb^+(Thr)	[N,CO,OH]	2.919,	3.129,	2.997,	54.1,	56.4,	66.5,	0.0 (2.4)	2.3 (5.5)	0.0 (0.0)
		2.854	*3.070*[e]	*2.948*	*55.3*[e]	*57.3*[e]	*67.6*	*0.0 (0.0)*	*0.2 (3.5)*	*0.0 (0.0)*
	[COOH]	2.902,	3.099,		43.3,			0.9 (0.0)	0.0 (0.0)	10.2 (6.9)
		2.822	*3.064*[f]		*44.0*[f]			*3.4 (0.1)*	*0.0 (0.0)*	*9.8 (6.5)*
	[CO_2^-]	2.891,	2.935,		45.5,			8.1 (8.9)	6.5 (8.2)	19.3 (17.8)
		2.810	*2.879*[f]		*46.6*[f]			*9.2 (10.0)*	*5.2 (7.0)*	*14.6 (13.1)*
	[N,CO]	2.819	3.176[e]		54.7[e]			12.6 (11.9)	14.6 (14.8)	20.6 (17.6)
	[CO,OH]	2.756		3.039			60.9	14.2 (13.6)	15.0 (15.3)	23.2 (20.3)
Rb^+(Pro)	[CO_2^-]	2.869,	2.963,		45.4,			0.0 (0.0)	0.0 (0.0)	0.0 (0.0)
	C3up	*2.793*	*2.900*[f]		*46.5*[f]			*0.0 (0.0)*	*0.0 (0.0)*	*0.0 (0.0)*
	[CO_2^-]	2.866,	2.964,		45.5,			3.0 (3.4)	4.0 (4.4)	5.7 (6.1)
	C3down	*2.789*	*2.900*[f]		*46.6*[f]			*3.1 (3.5)*	*4.2 (4.6)*	*5.4 (5.8)*
	[COOH]	2.886,	3.171,		42.8,			6.5 (8.6)	5.3 (7.4)	6.3 (8.4)
	C3up	*2.812*	*3.112*[f]		*43.7*[f]			*7.3 (9.4)*	*6.0 (8.1)*	*8.7 (10.8)*
	[COOH]	2.887,	3.166,		42.8,			7.9 (10.1)	7.4 (9.6)	9.4 (11.6)
	C3down	*2.808*	*3.139*[f]		*43.4*[f]			*9.1 (11.3)*	*8.5 (10.7)*	*11.9 (14.1)*
	[N,CO]	2.924	3.190[e]		56.0[e]			20.1	22.6	18.3
	[CO]	2.778						52.2	55.9	57.3

[a] Structures calculated at the B3LYP/HW*/6-311+G(d,p) (roman) or B3LYP/Def2TZVP (italics) level of theory. [b] Carbonyl oxygen of the amino acid backbone. [c] Hydroxyl oxygen of the amino acid side chain. [d] Relative free energies at 0 (298) K determined at the indicated level of theory with the HW*/6-311+G(2d,2p) (roman) or Def2TZVP (italics) basis sets using the associated B3LYP geometry. [e] X = amino nitrogen. [f] X = hydroxyl oxygen of the amino acid backbone.

complex collapses to the [CO]cc ground state conformer. Finally, a high lying conformer in which the metal ion binds only to the amino group, [N]tt, was located 43−50 kJ/mol above the GS.

The Rb^+(Ser) and Rb^+(Thr) complexes have very similar metal−ligand bond distances for all analogous conformers. Calculations identify the GS conformer as the tridentate [N,CO,OH], with the bidentate [COOH] conformer lying 1−5 (B3LYP) and 10−11 (MP2) kJ/mol higher in energy. In contrast, the B3P86 calculations generally find that the [COOH] conformer in which the metal ion binds to both oxygen atoms of the carboxylic acid group is the GS, with [N,CO,OH] lying 0.2−2.3 kJ/mol higher in energy (except for the Def2TZVP results for Rb^+(Ser) where the order is inverted). The [CO_2^-] zwitterionic analogue of [COOH] is found to lie 5−9 kJ/mol above [COOH]. Two bidentate conformers, [N,CO] and [CO,OH], where the metal ion binds to the side-chain hydroxyl in the latter, are found to lie 11−14 kJ/mol above the [N,CO,OH] GS conformer at the DFT level of theory and 20−23 kJ/mol at the MP2(full) level.

For Rb^+(Pro), the zwitterionic structure is the clear ground state, with [CO_2^-]C3up the lowest energy conformer at all levels of theory. The very similar [CO_2^-]C3down conformer (Figure 2) is only 3−6 kJ/mol higher in energy. The metal−oxygen bond distances in these two conformers are nearly identical, such that the energetic difference appears to lie primarily in a slightly shorter NH···OC hydrogen bond, 1.734 (1.738) versus 1.777 (1.781) Å using the Def2TZVP (HW*/6-311+G(d,p)) basis sets. The analogous [COOH] conformers lie higher in energy by 5−9 kJ/mol for C3up and 3−7 kJ/mol for C3down. Bidentate [N,CO] and [CO] conformers were also located but lie considerably higher in energy, 18−23 and 52−57 kJ/mol above the GS, respectively.

Compared to the lighter alkali metals, the ground state conformers for rubidium are generally the same as those found for potassium,[10,12,13] although there are some subtle distinctions. K^+(Gly) shows distinct [CO]cc and [COOH]cc conformations at several levels of theory, with energetic differences of ≤3 kJ/mol,[10] whereas the [COOH]cc conformer of Rb^+(Gly) collapses to [CO]cc. The [N,CO]tt conformer of K^+(Gly) lies closer in energy, only 1−7 kJ/mol above the GS. For Li^+(Gly) and Na^+(Gly),[9] the [N,CO]tt conformer is the clear GS. For the Ser and Thr complexes,[12,15,16] the lighter alkali ions all prefer the tridentate [N,CO,OH] conformers, with the [COOH] and [CO_2^-] structures increasing in excitation energy as the metal ion gets smaller. For proline, all metal ions prefer the zwitterionic structure because the secondary nitrogen is such a good proton acceptor.[13]

Conversion from 0 to 298 K and Excited Conformers. Conversion from 0 K bond energies to 298 K bond enthalpies and free energies is accomplished using the rigid rotor/harmonic oscillator approximation with rotational constants and vibrational frequencies calculated at the B3LYP/HW*/6-311+G(d,p) level. The resulting ΔH_{298} and ΔG_{298} values along with the conversion factors and 0 K enthalpies measured here for ground state conformers of all four Rb^+(AA) complexes are reported in Table 3. The uncertainties listed are determined by scaling most of the vibrational frequencies by ±10% along with 2-fold variations in the rubidium−ligand frequencies.

We also calculated the relative ΔG_{298} values for the four to eight lowest energy structures of these complexes, as listed in Table 2. In general, the relative ΔG_{298} excitation energies are comparable to the analogous differences in the ΔH_0 values, although variations up to ~3 kJ/mol can occur. Using the ΔG_{298} values to calculate an equilibrium population of conformers shows that the calculated [CO]cc ground state structure for Rb^+(Gly) should be dominant in the room temperature ion source, with the [N,CO]tt excited conformer calculated to comprise 2−27% of the total ion population. For Rb^+(Pro), the [CO_2^-]C3up ground state is the dominant conformer (77−88%), with [CO_2^-]C3down contributing 8−20% and the [COOH] conformers adding only 4−6%. For Rb^+(Ser) and Rb^+(Thr), the results depend drastically on the level of theory. The [N,CO,OH] conformers comprise 33−96 and 56−99%, respectively, with the [COOH] conformers contributing 4−63 and 1−38%, respectively, and [CO_2^-] conformers adding <4% and <6%, respectively. To investigate the effect of having a different conformer populating the Rb^+(AA) cations generated in the flow tube ion source, we analyzed the data using the molecular parameters of the two lowest energy conformers. The threshold energies change by less than 1 kJ/mol, and this effect is included in the uncertainties listed in the tables. The possibility of having a distribution of conformers is effectively included as the thermal distribution of internal energies available to the reactant ions.

TABLE 3: Enthalpies and Free Energies of Rubidium Cation Binding at 0 and 298 K (kJ/mol)[a]

complex	ΔH_0[b]	$\Delta H_{298}-\Delta H_0$[c]	ΔH_{298}	$T\Delta S_{298}$[c]	ΔG_{298}
Rb^+(Gly)	108.9 (7.0)	1.1 (0.7)	110.0 (6.9)	27.5 (5.0)	82.5 (8.5)
Rb^+(Ser)	115.7 (4.9)	0.2 (1.0)	115.9 (4.9)	31.0 (5.1)	84.9 (7.1)
Rb^+(Thr)	122.1 (4.6)	0.7 (1.0)	122.8 (4.6)	28.9 (7.8)	93.9 (9.1)
Rb^+(Pro)	125.2 (4.5)	0.7 (0.8)	125.9 (4.5)	29.9 (4.3)	96.0 (6.2)

[a] Uncertainties in parentheses. [b] Experimental values from Table 1. [c] Calculated using standard formulas and molecular constants calculated at the B3LYP/HW*/6-311+G(d,p) level.

Discussion

Comparison of Theoretical and Experimental Bond Dissociation Energies. The theoretical BDEs for the Rb^+(AA) complexes, where AA = Gly, Ser, Thr, and Pro, calculated at several levels of theory are compared to the experimental values in Table 4. When the HW*/6-311+G(2d,2p) basis set is used, we find that all three theoretical methods (B3LYP, B3P86, and MP2) yield BDE values for Rb^+(AA) that are systematically lower than experiment when counterpoise corrected. These different levels of theory also span a considerable range, especially when counterpoise corrections are not included in the MP2(full) values. Overall, the B3LYP(cp), B3P86(cp), and MP2(full,cp) values differ from experiment by about 11 kJ/mol, whereas the higher MP2(full) values have a mean absolute deviation (MAD) of only 5 kJ/mol. In contrast, results at all levels of theory using the Def2TZVP basis set provide bond energies in good agreement with experiment, with MADs of about 3 kJ/mol (7 for the MP2(full) values excluding cp corrections). Overall, all three levels of theory using the Def2TZVP basis set with counterpoise corrections give comparable agreement with the experimental values. Most levels of theory provide the same trends in the relative BDEs, namely, Gly < Ser < Thr < Pro, in agreement with experiment. Changes in the relative energies calculated using the more accurate Def2TZVP approach are sufficiently small compared to the HW*/6-311+G(2d,2p) approach used previously that the conclusions regarding populated structures in our IRMPD studies of Rb^+(Ser) and Rb^+(Thr) are unaffected.[15,16]

Trends in Bond Energies: Metal Cation Identity and Side-Chain Substitutents. Metal cations interact with amino acids by electrostatic ion induced−dipole, ion−quadrupole, and

TABLE 4: Experimental and Theoretical Rubidium Cation Affinities at 0 K (kJ/mol)

complex	experiment[a]	B3LYP(cp)[b]	B3P86(cp)[b]	MP2(full,cp)[b]	MP2(full)[b]
Rb^+(Gly)	108.9(7.0)	97.4	100.9	93.2	99.2
		104.8	*107.9*	*102.7*	*108.2*
Rb^+(Ser)	115.7(4.9)	103.6	104.6	112.5	120.8
		112.9	*112.2*	*118.2*	*129.4*
Rb^+(Thr)	122.1(4.6)	106.7	109.0	109.0	123.0
		117.2	*116.3*	*119.7*	*131.1*
Rb^+(Pro)	125.2(4.5)	114.3	114.1	112.0	120.3
		120.7	*121.6*	*122.4*	*130.9*
MAD[c]		12 (2)	11 (2)	11 (6)	5 (4)
		4 (1)	*3 (2)*	*3 (2)*	*7 (5)*

[a] Present experimental values from Table 1. Uncertainties in parentheses. [b] Calculations performed at the stated level of theory using a HW*/6-311+G(2d,2p) basis set with geometries and vibrational frequencies calculated at the B3LYP/HW*/6-311+G(d,p) level. Values in italics use the Def2TZVP basis set on all atoms with geometries and vibrational frequencies calculated at the B3LYP/Def2TZVP level. Counterpoise corrected (cp). [c] Mean absolute deviation from experimental values.

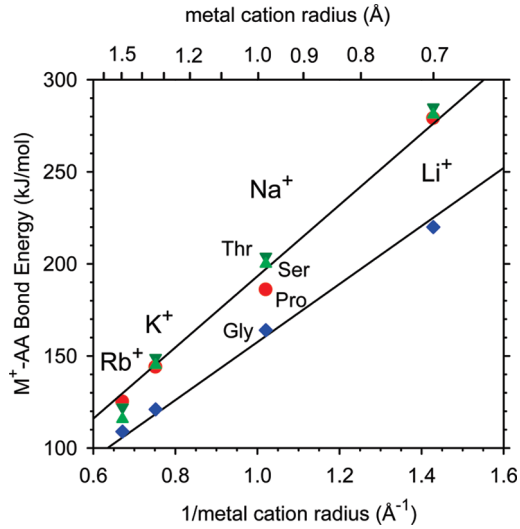

Figure 3. Experimental 0 K bond dissociation energies (in kJ/mol) for M^+(Gly) (blue diamonds), M^+(Pro) (red circles), M^+(Ser) (light green triangles), and M^+(Thr) (dark green inverted triangles) for $M^+ = Li^+$, Na^+, K^+, and Rb^+ are plotted versus the inverse metal cation radius (in $Å^{-1}$). The lines are linear regression fits to the M^+(Gly) and M^+(Ser) data constrained to pass through the origin.

ion−dipole forces that lead to solvation of the charge by coordination of the functional groups of the amino acids. Our results for the BDEs required to remove the rubidium cation from Rb^+(AA), where AA = Gly, Ser, Thr, Pro (Table 4), are smaller than the values for analogous complexes with $M^+ = Li^+$, Na^+, and K^+.[9−13] Indeed, the bond energies decrease systematically from Li^+ to Rb^+ because the electrostatic interactions decrease with the increasing bond distances necessitated by the increasing size of the metal cation (0.70, 0.98, 1.33, and 1.49 Å, respectively[69]). For the four amino acids studied here, this effect is clearly shown in Figure 3, which shows that the 0 K bond energies increase approximately linearly as the inverse of the ionic radius. (Note that such a dependence could imply a Coulombic potential; however, the true interactions must be combinations of ion−dipole (r^{-2}), ion−quadrupole (r^{-3}), and ion−induced dipole (r^{-4}) forces along with complex chelation effects.) The lines shown in Figure 3 are linear regression fits (constrained to pass through the origin) for the Gly and Ser data, where similar fits to the Pro and Thr data lie just below and just above, respectively, the Ser correlation. Slopes for the Gly, Pro, Ser, and Thr complexes are 158 ± 6, 190 ± 10, 193 ± 14, and 198 ± 10 Å kJ/mol, respectively. On average, the Pro, Ser, and Thr amino acids bind more strongly than Gly by 21 ± 8, 23 ± 10, and 25 ± 8%, respectively. As demonstrated elsewhere, Pro binds more strongly than Gly primarily because it has a higher polarizability.[8] Ser and Thr bind more strongly than Gly because the addition of the functionalized side chain provides a third binding site.[12] Figure 3 shows that the BDEs for Rb^+(Gly) and Rb^+(Pro) follow the trends established by the other metal cations reasonably well, consistent with the hypothesis regarding polarizability. In contrast, those for Rb^+(Ser) and Rb^+(Thr) are weaker than might be expected on the basis of the lighter metal cations. This suggests that the larger Rb^+ cation is unable to take full advantage of the tridentate binding associated with the functionalized side chains of these two amino acids.

This hypothesis can be verified by examining the metal−ligand bond lengths calculated for these complexes as a function of the metal cation identity. We find that they increase linearly with the metal cation radius with an intercept (cation radius = 0 Å) of 1.1−1.2 Å for all complexes. For the metal−carbonyl bond lengths associated with the [N,CO]tt geometry of Gly, the [N,CO,OH] geometries of Ser and Thr, and the [CO_2^-] geometry of Pro, the correlations increase linearly with slopes of 1.10−1.14, i.e., close to a slope of unity that would exactly match the increase with cation radius. In contrast, the metal−ligand distances for the other binding sites increase more rapidly with the cation radius: slopes of 1.18 for the other M−O bond in [CO_2^-] of Pro; 1.26 for the M−N and M−OH bonds in [N,CO,OH] of Ser and Thr; and 1.38 for M−N in [N,CO]cc of Gly. As demonstrated previously for Na^+ and K^+,[9,10] the carbonyl is the most strongly binding site in amino acids and therefore the M−OC bond lengths most closely follow the cation radius. The weaker amino and hydroxyl binding sites[9,10] increase more rapidly because the multidentate nature of the binding limits the ability of the ions to bind equivalently at all sites. In particular, the trend in M−N bond strengths for the [N,CO]tt conformer of M^+(Gly) results in a change in the predicted GS conformer from [N,CO]tt for $M^+ = Li^+$ and Na^+ to [CO]cc for $M^+ = K^+$ and Rb^+.

Conclusion

The kinetic energy dependences of the collision-induced dissociation (CID) of Rb^+(AA), where AA = Gly, Ser, Thr, and Pro, are examined in a guided ion beam tandem mass spectrometer. The only dissociation pathway observed is loss of the intact amino acid from the complex. Rb^+(AA) BDEs at 0 and 298 K for these complexes are obtained by detailed modeling of the experimental cross sections. The thresholds for binding to the amino acids follow the order of Rb^+(Gly) < Rb^+(Ser) < Rb^+(Thr) < Rb^+(Pro), in agreement with quantum

chemical calculations. When the basis set used is Def2TZVP, three different levels of theory including zero point energy corrections and counterpoise corrections for basis set superposition errors agree well with our experimental values, Table 4. Use of the HW*/6-311+G(2d,2p) basis set yields BDEs that are systematically low by about 11 kJ/mol.

The binding energies for these four amino acids to the alkali cations, Li^+, Na^+, K^+, and Rb^+, exhibit the expected trend that they decrease as the metal cation increases in size. A good correlation between these BDEs and the inverse of the atomic radius of the metal cation is found, although the Rb^+ binding affinities for Ser and Thr are slightly lower than would be expected on the basis of this correlation. This suggests that the larger rubidium cation cannot take advantage of the tridentate binding associated with the ground state conformers for these two amino acids, a result that seems likely for other amino acids having functionalized side chains. Examination of the detailed theoretical geometries of all complexes provides further insight into the origins of these trends.

Acknowledgment. This work is supported by the National Science Foundation, CHE-0748790 and CHE-0649039. A grant of computer time from the Center for High Performance Computing at the University of Utah is gratefully acknowledged.

References and Notes

(1) Hood, S. L.; Comar, C. L. *Arch. Biochem. Biophys.* **1953**, *45*, 423–433.
(2) Beauge, L. A.; Sjodin, R. A. *J. Physiol.* **1968**, *194*, 104–123.
(3) Matsuda, H.; Matsuura, H.; Noma, A. *J. Physiol.* **1989**, *413*, 139–157.
(4) Spruce, A. E.; Standen, N. B.; Stanfield, P. R. *J. Physiol.* **1989**, *411*, 597–610.
(5) Relman, S. R.; Lambie, A. T.; Burrows, B. A.; Roy, A. M. *J. Clin. Invest.* **1957**, *36*, 1249–1256.
(6) Richmond, C. R. *Health Phys.* **1980**, *38*, 1111–1153.
(7) Yen, C. K.; Budinger, T. F. *J. Comput.-Assisted Tomogr.* **1982**, *5*, 792–799.
(8) Rodgers, M. T.; Armentrout, P. B. *Acc. Chem. Res.* **2004**, *37*, 989–998.
(9) Moision, R. M.; Armentrout, P. B. *J. Phys. Chem. A* **2002**, *106*, 10350–10362.
(10) Moision, R. M.; Armentrout, P. B. *Phys. Chem. Chem. Phys.* **2004**, *6*, 2588–2599.
(11) Rodgers, M. T.; Armentrout, P. B. *Int. J. Mass Spectrom.* **2007**, *267*, 167–182.
(12) Ye, S. J.; Clark, A. A.; Armentrout, P. B. *J. Phys. Chem. B* **2008**, *112*, 10291–10302.
(13) Moision, R. M.; Armentrout, P. B. *J. Phys. Chem. A* **2006**, *110*, 3933–3946.
(14) Kapota, C.; Lemaire, J.; Maitre, P.; Ohanessian, G. *J. Am. Chem. Soc.* **2004**, *126*, 1836–1842.
(15) Armentrout, P. B.; Rodgers, M. T.; Oomens, J.; Steill, J. D. *J. Phys. Chem. A* **2008**, *112*, 2248–2257.
(16) Rodgers, M. T.; Armentrout, P. B.; Oomens, J.; Steill, J. D. *J. Phys. Chem. A* **2008**, *112*, 2258–2267.
(17) Ervin, K. M.; Armentrout, P. B. *J. Chem. Phys.* **1985**, *83*, 166–189.
(18) Muntean, F.; Armentrout, P. B. *J. Chem. Phys.* **2001**, *115*, 1213–1228.
(19) Moision, R. M.; Armentrout, P. B. *J. Am. Soc. Mass Spectrom.* **2007**, *18*, 1124–1134.
(20) Shaffer, S. A.; Prior, D. C.; Anderson, G. A.; Udseth, H. R.; Smith, R. D. *Anal. Chem.* **1998**, *70*, 4111–4119.
(21) Shaffer, S. A.; Tolmachev, A.; Prior, D. C.; Anderson, G. A.; Udseth, H. R.; Smith, R. D. *Anal. Chem.* **1999**, *71*, 2957–2964.
(22) Ye, S. J.; Armentrout, P. B. *J. Phys. Chem. A* **2008**, *112*, 3587–3596.
(23) Heaton, A. L.; Moision, R. M.; Armentrout, P. B. *J. Phys. Chem. A* **2008**, *112*, 3319–3327.
(24) Carl, D. R.; Moision, R. M.; Armentrout, P. B. *Int. J. Mass Spectrom.* **2007**, *265*, 308–325.
(25) Gerlich, D. *Adv. Chem. Phys.* **1992**, *82*, 1–176.
(26) Aristov, N.; Armentrout, P. B. *J. Phys. Chem.* **1986**, *90*, 5135–5140.
(27) Dalleska, N. F.; Honma, K.; Sunderlin, L. S.; Armentrout, P. B. *J. Am. Chem. Soc.* **1994**, *116*, 3519–3528.
(28) Daly, N. R. *Rev. Sci. Instrum.* **1960**, *31*, 264–267.
(29) Beyer, T. S.; Swinehart, D. F. *Commun. Assoc. Comput. Machinery* **1973**, *16*, 379.
(30) Stein, S. E.; Rabinovich, B. S. *J. Chem. Phys.* **1973**, *58*, 2438–2445.
(31) Stein, S. E.; Rabinovich, B. S. *Chem. Phys. Lett.* **1977**, *49*, 183–188.
(32) Hales, D. A.; Lian, L.; Armentrout, P. B. *Int. J. Mass Spectrom. Ion Processes* **1990**, *102*, 269–301.
(33) Robinson, P. J.; Holbrook, K. A. *Unimolecular Reactions*; Wiley Interscience: New York, 1972.
(34) Gilbert, R. G.; Smith, S. C. *Theory of Unimolecular and Recombination Reactions*; Blackwell Scientific: London, 1990.
(35) Truhlar, D. G.; Garrett, B. C.; Klippenstein, S. J. *J. Phys. Chem.* **1996**, *100*, 12771–12800.
(36) Loh, S. K.; Hales, D. A.; Lian, L.; Armentrout, P. B. *J. Chem. Phys.* **1989**, *90*, 5466–5485.
(37) Khan, F. A.; Clemmer, D. E.; Schultz, R. H.; Armentrout, P. B. *J. Phys. Chem.* **1993**, *97*, 7978–7987.
(38) Rodgers, M. T.; Ervin, K. M.; Armentrout, P. B. *J. Chem. Phys.* **1997**, *106*, 4499–4508.
(39) Meyer, F.; Khan, F. A.; Armentrout, P. B. *J. Am. Chem. Soc.* **1995**, *117*, 9740–9748.
(40) Rodgers, M. T.; Armentrout, P. B. *J. Phys. Chem. A* **1997**, *101*, 1238–1249.
(41) Koizumi, H.; Armentrout, P. B. *J. Am. Soc. Mass Spectrom.* **2001**, *12*, 480–489.
(42) Ye, S. J.; Moision, R. M.; Armentrout, P. B. *Int. J. Mass Spectrom.* **2006**, *253*, 288–304x.
(43) More, M. B.; Ray, D.; Armentrout, P. B. *J. Phys. Chem. A* **1997**, *101*, 831–839.
(44) More, M. B.; Ray, D.; Armentrout, P. B. *J. Phys. Chem. A* **1997**, *101*, 4254–4262.
(45) More, M. B.; Ray, D.; Armentrout, P. B. *J. Phys. Chem. A* **1997**, *101*, 7007–7017.
(46) Ye, S. J.; Armentrout, P. B. *J. Phys. Chem. A* **2008**, *112*, 3587–3596.
(47) Rodgers, M. T.; Armentrout, P. B. *J. Chem. Phys.* **1998**, *109*, 1787–1800.
(48) Waage, E. V.; Rabinovitch, B. S. *Chem. Rev.* **1970**, *70*, 377–387.
(49) Armentrout, P. B.; Simons, J. *J. Am. Chem. Soc.* **1992**, *114*, 8627–8633.
(50) Becke, A. D. *J. Chem. Phys.* **1993**, *98*, 5648–5652.
(51) Lee, C.; Yang, W.; Parr, R. G. *Phys. Rev. B* **1988**, *37*, 785–789.
(52) McLean, A. D.; Chandler, G. S. *J. Chem. Phys.* **1980**, *72*, 5639–5648.
(53) Heaton, A. L.; Armentrout, P. B. *J. Phys. Chem. B* **2008**, *112*, 12056–12065.
(54) Heaton, A. L.; Bowman, V. N.; Oomens, J.; Steill, J. D.; Armentrout, P. B. *J. Phys. Chem. A* **2009**, *113*, 5519–5530.
(55) Hay, P. J.; Wadt, W. R. *J. Chem. Phys.* **1985**, *82*, 299–310.
(56) Glendening, E. D.; Feller, D.; Thompson, M. A. *J. Am. Chem. Soc.* **1994**, *116*, 10657–10669.
(57) Foresman, J. B.; Frisch, A. E. *Exploring Chemistry with Electronic Structure Methods*, 2nd ed.; Gaussian, Inc.: Pittsburgh, PA, 1996.
(58) Boys, S. F.; Bernardi, R. *Mol. Phys.* **1970**, *19*, 553–566.
(59) van Duijneveldt, F. B.; van Duijneveldt-van de Rijdt, J. G.; C, M.; van Lenthe, J. H. *Chem. Rev.* **1994**, *94*, 1873–1885.
(60) Hoyau, S.; Norrman, K.; McMahon, T. B.; Ohanessian, G. *J. Am. Chem. Soc.* **1999**, *121*, 8864–8875.
(61) Feller, D.; Glendening, E. D.; Woon, M. W.; Feyereisen, J. *J. Chem. Phys.* **1995**, *103*, 3526.
(62) Feller, D. *Chem. Phys. Lett.* **2000**, *322*, 543.
(63) McMahon, T. B.; Ohanessian, G. *Chem.—Eur. J.* **2000**, *6*, 2931–2941.
(64) Weigend, F.; Ahlrichs, R. *Phys. Chem. Chem. Phys.* **2005**, *7*, 3297.
(65) Leininger, T.; Nicklass, A.; Kuechle, W.; Stoll, H.; Dolg, M.; Bergner, A. *Chem. Phys. Lett.* **1996**, *255*, 274–280.
(66) Feller, D. *J. Comput. Chem.* **1996**, *17*, 1571–1586.
(67) Schuchardt, K. L.; Didier, B. T.; Elsethagen, T.; Sun, L.; Gurumoorthi, V.; Chase, J.; Li, J.; Windus, T. L. *J. Chem. Inf. Model.* **2007**, *47*, 1045–1052.
(68) Lifshitz, C. *Adv. Mass Spectrom.* **1989**, *11*, 713–729.
(69) Wilson, R. G.; Brewer, G. R. *Ion Beams with Applications to Ion Implantation*; Wiley: New York, 1973.

JP101264M